Strong configuration interaction in the 3*p* photoelectron spectrum of Kr

S. Kosugi,[1,2] F. Koike,[1] T. Nagayasu,[2,3] F. Hosseini,[4,5] J. Martins,[4] T. Marchenko,[4] O. Travnikova,[4] M. Oura,[2] T. Gejo,[2,3] J. R. Harries,[6] J. D. Bozek,[5] K. Ito,[5] E. Sokell,[7] S. Fritzsche,[8,9] M. N. Piancastelli,[4,10] M. Simon,[4] and Y. Azuma[1,2]

[1]*Department of Materials and Life Sciences, Sophia University, Tokyo 102–8554, Japan*
[2]*RIKEN SPring-8 Center, 1-1-1 Kouto, Sayo-cho, Sayo-gun, Hyogo 679–5148, Japan*
[3]*Graduate School of Materials Science, University of Hyogo, Kamigori-cho, Ako-gun 678–1297, Japan*
[4]*Sorbonne Universités, CNRS, UMR 7614, Laboratoire de Chimie Physique-Matière et Rayonnement, F-75005 Paris, France*
[5]*Synchrotron SOLEIL, L'Orme des Merisiers, Saint-Aubin, BP 48, F-91192 Gif-sur-Yvette Cedex, France*
[6]*National Institutes for Quantum and Radiological Science and Technology, SPring-8, 1-1-1 Kouto, Sayo, Hyogo 679–5148, Japan*
[7]*School of Physics, University College Dublin, Dublin 4, Belfield, Ireland*
[8]*Helmholtz-Institut Jena, Fröbelstieg 3, D-07743 Jena, Germany*
[9]*Theoretisch-Physikalisches Institut, Friedrich-Schiller-Universität Jena, Max-Wien-Platz 1, D-07743 Jena, Germany*
[10]*Department of Physics and Astronomy, Uppsala University, Box 516, SE-75120 Uppsala, Sweden*

(Received 5 November 2019; accepted 3 March 2020; published 8 April 2020)

We measured the Kr photoelectron spectrum in the region close to the $3p$ ionization threshold. Our high-resolution measurements allowed a clear observation of spectral structures due to electron correlation effects. Analysis based on relativistic multiconfiguration calculations could explain these observed peaks as due to strong configuration interactions between the $3p^{-1}$ state and $3d^{-2}nl$ states. Calculated and experimental data for peak assignments and intensity distributions are in good agreement. In addition, we measured the anisotropy parameter β, which also agreed well with theory. These findings provide a detailed view of strong configuration interactions between the $3p^{-1}$ and $3d^{-2}nl$ inner-shell hole states.

DOI: 10.1103/PhysRevA.101.042505

I. INTRODUCTION

Inner-shell vacancy states of an atom may strongly interact with other configurations of the same symmetry due to electron correlation effects. As a result, several additional peaks may arise as satellites to the main (photo) peak in the photoelectron spectrum due to other final ionic states with the same symmetry. These lines may be assigned as "correlation satellites" [1–3]. The correlation satellites can be classified as "dipole correlation satellites" [2] or "monopole correlation satellites" depending on the combination of constituent single-electron orbitals, and the latter is historically referred also as "shake satellites." Clear correlation satellite spectra were observed in the photoionization of subvalence shell of rare gases such as Ne 2*s* [4–7], Ar 3*s* [4–8], Kr 4*s* [4–6,9–11], and Xe 5*s* [4–6,10,11]. We can further refer to Ref. [12] for various cases of correlation satellites. They were also observed in cases of deep inner-shell ionization. Correlation satellite spectra by photoionization of Ne 1*s*, Ar 2*p*, Kr 3*p*, and Kr 3*d* were reported by Svensson *et al.* [4,13], although the experimental resolution was not high enough to identify and explain the detailed structure of the satellites. However, a general trend was indicated that the number of correlation satellites increase with the atomic number (Z) as the number of available electrons increases. Moreover, the presence of correlation satellites also in molecules containing high-Z elements (starting from the third row of the Periodic Table of Elements), leads to decrease in the intensity of the main photoelectron line, which consequently causes deviations of measured photoelectron peak intensities from expected stoichiometric ratios [1].

In the $3p$ photoionization process, the $3p$ vacancy ionic states are strongly modified due to electron correlation effects. Ohno and Wendin [14,15] have pointed out that this $3p$ vacancy interacts strongly with $3d^{-2}$ ($3d$ double-vacancy) configurations and may cause super-Coster-Kronig transitions [16]. Svensson *et al.* [4,13] have measured Kr $3p$ photoelectron spectrum using Al K_α radiation, and discussed the importance of configuration interaction with $3d^{-2}nl$ states in order to understand the Kr $3p$ core lines.

Our measurements of Kr^+ $3d^{-2}nl$ correlation satellite lines were carried out with a high-resolution hemispherical electron analyzer using synchrotron radiation. As a result, we were able to confirm detailed spectral structures related to $Kr^+3d^{-2}nl$ states. We have also measured the angular distribution and obtained the beta values for these spectral lines. To understand the experimental spectral features and to evaluate the role of electron correlations in the photoionization processes, a set of fully relativistic multiconfiguration calculations have been performed. Our calculations predict that the $3p$ vacancy states contain the $3d$ double-vacancy configurations, where one state may be represented in terms of the linear combination of $3p^{-1}$ and $3d^{-2}np$ (with $n = 5$, 6, or more) configurations. This configuration mixing causes modification of the photoionization spectral peaks and the appearance of correlation satellites. The $3d^{-2}np$ levels that mix with the $3p$ hole state are excited, borrowing intensity from the main $3p^{-1}$ photoexcitation.

We briefly introduce our method and procedure of our experiment in the next section. In Sec. III, we describe our theoretical calculations. In Sec. IV, we discuss the result of

our experiments and calculations and finally, we give some concluding remarks in Sec. V.

II. EXPERIMENT

Initial exploratory experiments were performed at the x-ray beamline BL17SU at SPring-8, an 8 GeV synchrotron radiation facility in Japan, and final measurements were made at the PLEIADES beamline of the 2.75 GeV French national synchrotron facility SOLEIL. The PLEIADES beamline is equipped with an HU80 undulator, delivering variable polarization (including linear horizontal and vertical, corresponding to 0° and 90° between the electric vector of the light and the electron detection) in the energy range between 15 and 900 eV, and a high-resolution monochromator employing varied-grooth-depth and varied-line-spacing gratings. Kinetic energies of the emitted electrons were measured by a hemispherical electron energy analyzer (VG Scienta R4000) mounted perpendicular to the propagation axis of the photon beam. The analyzer was used with a constant pass energy of 10 eV, resulting in a total experimental resolution of about 60 meV at 440 eV photon energy. The calibration of angular dependence of the efficiency of the analyzer was accomplished by Ne $2p$ photoelectron measurments. The measured Ne $2p$ intensities were normalized using the angular anisotropy parameters β from Ref. [17]. The photon energy scale and electron analyzer scale were calibrated by Kr $3d$ photoelectron [18] and Kr *MNN* Auger lines [19]. All photoelectron spectra were normalized with respect to the gas pressure, acquisition time, and photon flux, which were monitored continuously during measurements. Asymmetry parameters β were determined by obtaining the peak intensity ratio for parallel and perpendicular directions to the photon polarization, with the peaks fitted by the Voigt function.

III. THEORY

To understand the spectral features in the Kr $3p$ photoionization region, we performed a set of multiconfiguration Dirac-Fock calculations for the electronic structures of Kr ground state and for Kr^+ excited states in the Kr^+ $3p^{-1}\,{}^2P_{1/2,3/2}$ photoionization region by using the General Purpose Relativistic Atomic Structure Program 92 (GRASP92) [20] and also the RATIP package [21,22]. The photoelectron energies, photoionization cross sections, and anisotropy parameters β were calculated.

To obtain the wave function of the Kr ground state, we initially optimized the Kr $1s^22s^22p^63s^23p^63d^{10}4s^24p^6$ configuration. We then further evaluated the correlation contributions by means of the active-space method [23] including higher-lying orbitals with principal quantum numbers increasing stepwise from $n = 4$ to 8, in which all of the single and double electron excitations from $n = 3$ and 4 shells were considered and all of the higher-lying orbitals were treated as correlation orbitals. The effects of Breit interaction and QED corrections were included perturbatively in GRASP92. The total energies for the minimal basis state were calculated to be −75 825.37 eV and for the states with correlation relaxation they became −75 845.90 eV if single and double virtual excitations up to $n = 8$ were included. Good convergence was achieved for these total energies. The correlation contribution from $n = 3$ and 4 shells to the Kr ground state was then evaluated to be −20.53 eV. For all further computations of the photoionization amplitudes and dynamics, however, we just applied the minimal basis-state wave functions for the calculation of photoionization dynamics to avoid the complexity in the evaluation of core relaxation contributions to the Kr^+ $3p$ hole states. Because the core relaxation effects are slightly different between the ground and $3p$ hole states, the present treatment may cause a systematic error for the evaluation of excitation energies. This error can be expected to be much smaller than the total present correlation contribution of −20.53 eV. A systematic error of 2.41 eV was found by comparison to the experimental data.

To calculate the Kr^+ $3p$ hole state, we first optimized the states of $1s^22s^22p^63s^23p^53d^{10}4s^24p^6$ configuration with total angular momentum $J = 1/2$ and 3/2 simultaneously. We obtained the total energies −75 608.30 eV for $J = 3/2$ state and −75 600.30 eV for $J = 1/2$ state. The energy difference between the $J = 1/2$ and 3/2 states was 8.00 eV, in excellent agreement with the experiment. We also obtained the single-electron orbital binding energies in units of hartree (1 hartree = 27.211 eV). Those were 9.58 and 9.27 for $3p-$ ($3p$ spin-down) and $3p+$ ($3p$ spin-up) orbitals, respectively; 4.70 and 4.65 for $3d-$ ($3d$ spin-down) and $3d+$ ($3d$ spin-down) orbitals, respectively. We note that the statistically averaged value 4.67 $[=(4.70 \times 4 + 4.65 \times 6)/(4 + 6)]$ of the $3d$ orbital energies almost equals half of the statistically averaged value 9.37 $[=(9.58 \times 2 + 9.27 \times 4)/(2 + 4)]$ of the $3p$ orbital energies. This suggests that the energy for removing two $3d$ electrons from a Kr atom is roughly the same as those for ionizing a single $3p$ electron from the system, but the energy to remove multiple electrons from an atom is not rigorously an addition of single-electron orbital binding energies. When compared to the $3p$ hole configuration, therefore, the total electronic energy does not change by a large amount when we replace one $3d$ orbital by a $3p$ orbital and simultaneously another $3d$ orbital by a loosely bound Rydberg orbital such as np (with $n = 5$ or higher). In other words, the $3d$ double-hole Rydberg-state configuration $1s^22s^22p^63s^23p^63d^84s^24p^6np$ is almost degenerate with the $3p$ hole-state configuration $1s^22s^22p^63s^23p^53d^{10}4s^24p^6$. Both configurations will therefore interact strongly and modify the wave function because the degree of the configuration interaction is generally proportional to the inverse of the difference in configuration-state energy. As second and further steps we included the $1s^22s^22p^63s^23p^63d^84s^24p^6np$ configurations in the multiconfiguration Dirac-Fock procedure. The single-electron orbitals $5p$, $6p$, $7p$, and $8p$ were optimized successively by freezing the lower-lying orbitals. We included also the configurations $1s^22s^22p^63s^23p^63d^84s^24p^6nf$ with $n = 4$ to 8, which enabled us to evaluate the influence of nf orbitals to the electronic states and photoionization dynamics.

The $3p$ photoionization dynamics has been calculated by using the "Photo" component of the RATIP program [22]. This program enables using different single-electron orbital basis sets that are nonorthogonal between the initial and final states. The distorted wave with static exchange continuum wave function was generated in the program. We calculated the photoionization process for 440.8 eV linearly polarized

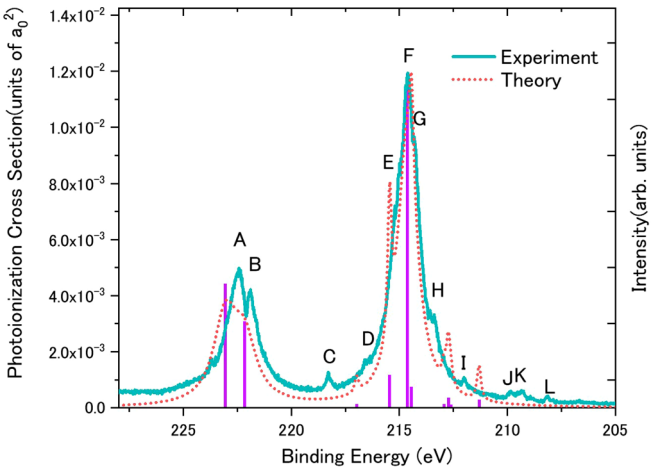

FIG. 1. Photoelectron spectrum above the Kr ionization threshold excited by 439.56 eV photons. The solid curve represents $I(0^\circ) + 2I(90^\circ)$ (see text). The corresponding assignments and binding energies are presented in Table I. Vertical bars are photoionization cross sections obtained from our calculation. The dashed curve is the theoretical spectrum obtained from convolution of the cross sections by corresponding core-hole lifetimes and experimental resolution.

incident photon in length form (Babushkin gauge) and also in a velocity form (Coulomb gauge). For these two gauges, the results differed by less than 13% in all the calculated photoionization cross sections. The mean value between these gauge forms are used below to display and compare the theoretical results with experiment. We also calculated the anisotropy parameters β for linearly polarized incident light. Also for β, both length and velocity form calculations were generated and found to differ by less than 0.3% for all photoionization peaks considered. In total, 174 spectral lines were calculated. The excitation energies, which are the energy differences between the Kr^+ states and the Kr ground state, contained a systematic shift due to the truncation error that arises from the insufficient evaluation of the core relaxation effects. Our calculation was adjusted to the experimental data at the peak of the $3p^{-1}$ $J = 3/2$ diagram line. All the theoretical energies have been shifted by 2.41 eV towards the higher-energy side. In Fig. 1, the experimental spectral intensity is normalized to the theoretical peak height of the $3p^{-1}$ $J = 3/2$ diagram line.

IV. RESULTS AND DISCUSSION

The photoelectron spectrum around the Kr $3p$ ionization threshold, excited by 439.56 eV photons, is presented in Fig. 1. We chose this incident energy (439.56 eV) since it is sufficiently higher than the $3p$ ionization energy (by about 220 eV: see Table I). Therefore, no peak deformation due to the Post-Collision Interaction (PCI) effect had to be considered [24]. The spectra were measured at angles of 0°and 90° with respect to the electric vector of the linearly polarized photon beam. The respective intensity distributions used to calibrate the angular dependence of the efficiency of the analyzer are denoted as $I(0^\circ)$, and $I(90^\circ)$. For comparison to theory, Fig. 1 also plots $I(0^\circ) + 2I(90^\circ)$, which is equivalent to the total cross section. The corresponding assignments and binding energies are presented in Table I. The vertical bars are cross sections obtained from our calculation. The dashed curve is the theoretical spectrum obtained from the convolution of the theoretical cross sections with a Voigt function. The Lorentzian full width at half maximum of 1.3 eV [25] for peak A and peak B, 1.1 eV [25] for peak F, which corresponds to the lifetime widths of the $3p_{1/2}$ and $3p_{3/2}$ hole states respectively, and 0.2 eV [18] (twice the lifetime width of the $3d_{5/2}$ hole state) were used for convolution of the other peaks. Gaussian contribution of 60 meV was used to account for line broadenings due to total experimental. The vertical scales for the experimental and theoretical spectra are normalized with peak F.

Experimental and theoretical binding energies and theoretical cross sections are listed in Table I. The leading two configurations are also listed with their percentage fractions. One of the remarkable features in the results can be seen from peaks A and B; the percentage fraction of the peak A is 57.4% from $3p^{-1}\,^2P_{1/2}$ and 40.4% from $3d^{-2}(^1S_0)5p\,^2P_{1/2}$ configurations whereas the peak B is 57.4% from $3d^{-2}(^1S_0)5p\,^2P_{1/2}$ and 40.3% from $3p^{-1}\,^2P_{1/2}$ configurations. These two are complete mixtures of two configurations $3p^{-1}\,^2P_{1/2}$ and $3d^{-2}(^1S_0)5p\,^2P_{1/2}$ with an energy difference of 0.89 eV. Because the excitation strengths to these states are almost exclusively due to $3p^{-1}\,^2P_{1/2}$ configuration, the ratio of photoionization cross sections is expected to be $57.4/40.3 = 1.42$ between the peaks A and B, which is in quite good agreement with the ratio of theoretical results 4.41×10^{-3} $a_0{}^2/3.07 \times 10^{-3}$ $a_0{}^2 = 1.44$ where $a_0{}^2$ is the square of the Bohr radius $a_0 (= 0.529 \times 10^{-8}$ cm). Moreover, as seen from the doublet structure at around 222 eV in Fig. 1, the $3p^{-1}\,^2P_{1/2}$ diagram line splits into two peaks due to the strong correlation interaction with $3d$ double-vacancy configurations. For the individual peaks J, K, L, neither theoretical binding energy nor cross section could be assigned. These peaks may be due to the admixture of other configurations, not explicitly related to the configuration interactions between $3p^{-1}$ and $3d^{-2}np$.

We have also obtained the values of the anisotropy parameter β by comparing the spectral intensities for photoelectrons detected parallel to and perpendicular to the incident photon linear polarization. In Fig. 2 and Table II, experimental β parameters are shown together with the results of the present theoretical calculations. Experimental β for the observed peaks are mainly scattered between 1.1 and 1.5 except for the peaks at lower binding energies. The β for the prominent peaks A, B, and F are 1.19, 1.18, and 1.22, respectively, in good agreement with the theoretical values, 1.29, 1.30, and 1.29. The major contribution to the photoionization is the direct dipole transition from the Kr ground-state configuration to the $3p^{-1}\,^2P_{1/2}ks$ or kd channels, where k is the wave number of the photoelectron, in both the direct and correlation ionization channels. In the correlation satellites, the excited states are actually the mixture of the $3p^{-1}\,^2P_{1/2}$ and $3d^{-2}(^1S_0)5p\,^2P_{1/2}$ configurations. Although the major effect to the energy shift comes from the $3d$ double-vacancy configurations, they have almost no contribution to the $3p$ vacancy configurations. The intensity borrowing [26] from the $3p^{-1}\,^2P_{1/2}$ configuration that is slightly mixed in the $3d^{-2}(^1S_0)5p\,^2P_{1/2}$ correlation satellite states therefore plays a decisive role for the appearance of the correlation satellite peaks, cf. also Ref. [27].

TABLE I. Binding energies, cross sections, and dominant configurations of the main states contributing to the observed features.

	Binding energy exp. (eV)	Binding energy theory (eV)[a]	Photoionization cross section theory ($10^{-2}a_0{}^2$)[b]	Dominant configuration admixtures (in %)			
A	222.44	223.062	0.441	57.4 $3p^5(^2P_{1/2})$	40.4 $3d^8(^1S_0)5p(^2P_{1/2})$		
B	221.90	222.172	0.307	57.4 $3d^8(^1S_0)5p(^2P_{1/2})$	40.3 $3p^5(^2P_{1/2})$		
C	218.30	218.517	0.001	96.8 $3d^8(^1G_2)4f(^2P_{3/2})$			
		218.493	0.001	37.5 $3d^8(^1D_2)7p(^2P_{1/2})$	28.4 $3d^8(^3P_2)7p(^2S_{1/2})$	7.4 $3d^8(^3P_2)7p(^4P_{1/2})$	3.8 $3d^8(^3G_2)7p(^4D_{3/2})$
D	216.50	216.980	0.013	32.6 $3d^8(^1D_2)7p(^2P_{3/2})$	15.9 $3d^8(^3P_2)7p(^4S_{3/2})$	15.4 $3d^8(^3P_2)7p(^2P_{3/2})$	13.2 $3d^8(^1D_2)7p(^2D_{3/2})$
E	215.20	215.454	0.118	23.9 $3d^8(^1D_2)6p(^2P_{3/2})$	12.3 $3d^8(^3P_2)6p(^4S_{3/2})$	12.3 $3d^8(^1D_2)6p(^2D_{3/2})$	11.0 $3d^8(^3P_2)6p(^2P_{3/2})$
F	214.63	214.630	1.185	72.9 $3p^5(^2P_{3/2})$			
G	214.35	214.452	0.042	48.5 $3d^8(^3F_2)7p(^4F_{3/2})$	32.1 $3d^8(^3F_2)7p(^4D_{3/2})$		
		214.446	0.021	44.0 $3d^8(^3F_2)7p(^2D_{3/2})$	31.8 $3d^8(^3F_2)7p(^4F_{3/2})$	12.6 $3d^8(^3F_2)7p(^4D_{3/2})$	
		214.384	0.016	45.7 $3d^8(^3F_2)8f(^2P_{3/2})$	25.2 $3d^8(^3F_2)8f(^2D_{3/2})$	13.5 $3d^8(^3F_2)8f(^4S_{3/2})$	
H	213.49	212.937	0.015	19.9 $3d^8(^3P_2)5p(^4S_{3/2})$	17.6 $3d^8(^3P_2)5p(^4P_{3/2})$	15.5 $3d^8(^1D_2)5p(^2P_{3/2})$	12.1 $3d^8(^3P_2)5p(^4D_{3/2})$
		212.741	0.036	18.2 $3d^8(^3P_2)5p(^2P_{3/2})$	17.3 $3d^8(^1D_2)5p(^2D_{3/2})$	15.7 $3d^8(^3P_2)5p(^2D_{3/2})$	12.7 $3d^8(^3P_2)5p(^4P_{3/2})$
		212.627	0.013	25.4 $3d^8(^3P_2)5p(^2D_{3/2})$	19.1 $3d^8(^3P_2)5p(^4P_{3/2})$	18.5 $3d^8(^3P_2)5p(^4D_{3/2})$	17.7 $3d^8(^1D_2)5p(^2P_{3/2})$
I	211.99	211.314	0.029	32.3 $3d^8(^1D_2)5p(^2P_{3/2})$	19.5 $3d^8(^1D_2)5p(^2D_{3/2})$	18.1 $3d^8(^3P_2)5p(^2P_{3/2})$	12.9 $3d^8(^3P_2)5p(^4S_{3/2})$
J	209.86						
K	209.31						
L	208.12						

[a]Our calculation was adjusted to the experimental data at the peak of the $3p^{-1}J = 3/2$ diagram line. All the theoretical energies have been shifted by 2.41 eV towards the higher-energy side.
[b]$a_0{}^2$ is the square of the Bohr radius $a_0(= 0.529 \times 10^{-8}$ cm).

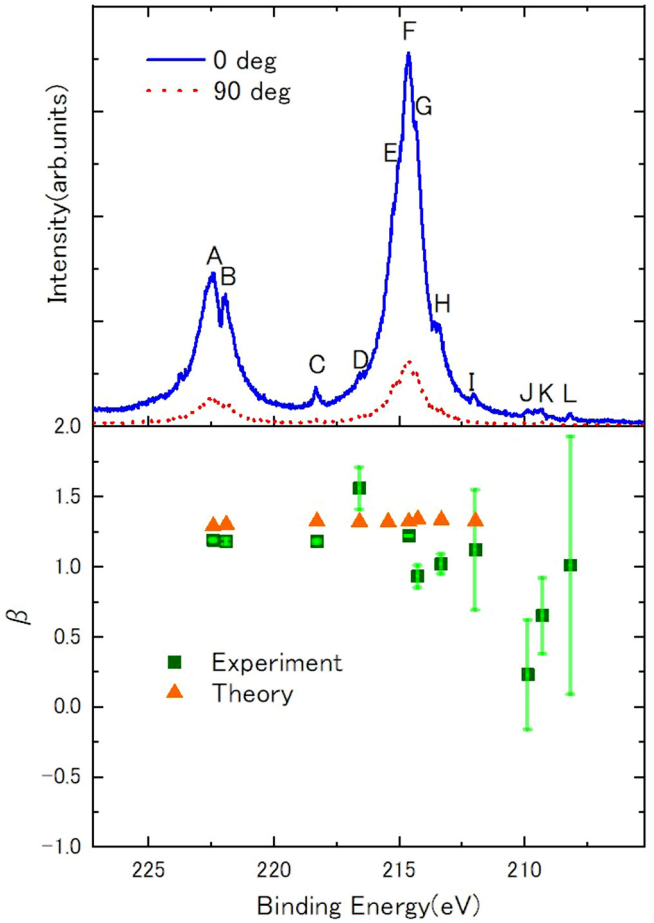

FIG. 2. Upper part: photoelectron spectrum around the Kr 3p ionization threshold with 439.56 eV photons measured at two emission angles, 0°(solid curve) and 90°(dotted curve). Lower part: experiment values of the β parameter for some of the peaks observed in the upper part of the figure. The results of theoretical calculations are also shown in the figure.

Theoretically, it is therefore reasonable to assume that both the diagram peaks and correlation satellite peaks have the same values for asymmetry parameters β . As found in Table II, the agreement of the β parameters supports the present argument, and also all the smaller peaks observed in this energy region can be verified as the $3d^{-2}(^1S_0)5p\,^2P_{1/2}$ correlation satellites.

V. CONCLUSION

Features due to strong configuration interactions in the Kr 3p inner shell were observed clearly by high-resolution photoelectron spectroscopy. Binding energies obtained by relativistic multiconfiguration calculations and detailed assignments of the Kr^+ $3d^{-2}nl$ correlation satellite lines are reported. The calculated cross sections of each state reproduced the intensity distribution of the experimental spectrum quite well. The anisotropy parameter β was obtained by angle-resolved measurements. Our theoretical calculations are in good agreement with the experimental β values. Our theoretical calculation did not reproduce the experimentally observed peaks *J, K*, and *L*. They present a challenge for further theoretical investigations.

TABLE II. Binding energies and anisotropy parameter β for the main states measured. The theoretical values of β are the average values of the calculated results in length form and in velocity form. (The percentage differences between the results of both forms were less than 0.3% for all of the photoionization peaks calculated.)

	Binding energy Exp. (eV)	Binding energy Theory (eV)	β Exp.	β Theory
A	222.44	223.062	1.19 ± 0.01	1.29
B	221.90	222.172	1.18 ± 0.02	1.30
C	218.30	218.517	1.18 ± 0.01	1.32
		218.493		1.33
D	216.50	216.980	1.56 ± 0.15	1.33
E	215.20	215.454		1.33
F	214.63	214.630	1.22 ± 0.01	1.29
G	214.35	214.452	0.93 ± 0.08	1.34
		214.446		1.34
		214.384		1.34
H	213.49	212.937	1.02 ± 0.07	1.33
		212.741		1.33
		212.627		1.34
I	211.99	211.314	1.12 ± 0.43	1.33
J	209.86		0.23 ± 0.39	
K	209.31		0.65 ± 0.27	
L	208.12		1.01 ± 0.92	

ACKNOWLEDGMENTS

This material is based on work supported by the Japan Society for the Promotion of Science through Grants-in-Aid for Scientific Research Category “C,” Grants No. 23600009, and No. 17K05600. The authors are grateful to the technical staff of BL17SU of SPring-8 for assistance beamtime under the approval of RIKEN Proposal No. 20170028. We are also grateful to the SOLEIL staff for operating the facility and providing beamtime under Project No. 20181268.

[1] O. Travnikova, M. Patanen, J. Söderström, A. Linblad, J. J. Kas, F. D. Vila, D. Céolin, T. Marchenko, G. Goldsztejn, R. Guillemin, L. Journel, T. X. Carroll, K. J. Børve, P. Decleva, J. J. Rehr, N. Mårtensson, M. Simon, S. Svensson, and L. J. Sæthre, J. Phys. Chem. A **123**, 7619 (2019).

[2] G. Wendin and M. Ohno, Phys. Scr. **14**, 148 (1976).

[3] G. Wendin, *Breakdown of One-electron Pictures in Photoelectron Spectra, Structure and Bonding* (Springer, Heidelberg, 1981), Vol. 45.

[4] S. Svensson, B. Eriksson, N. Mårtensson, G. Wendin, and U. Gelius, J. Electron Spectrosc. Relat. Phenom. **47**, 327 (1988).

[5] M. O. Krause, S. B. Whitfield, C. D. Caldwell, J. Z. Wu, P. van der Meulen, C. A. de Lange, and R. W. C. Hansen, J. Electron Spectrosc. Relat. Phenom. **58**, 79 (1992).
[6] A. Kikas, S. J. Osborne, A. Ausmees, S. Svensson, O. P. Sairanen, and S. Aksela, J. Electron Spectrosc. Relat. Phenom. **77**, 241 (1996).
[7] U. Becker and D. Shirley, Phys. Scr. **T31**, 56 (1990).
[8] U. Becker, B. Langer, H. G. Kerkhoff, M. Kupsch, D. Szostak, R. Wehlitz, P. A. Heimann, S. H. Liu, D. W. Lindle, T. A. Ferrett, and D. A. Shirley, Phys. Rev. Lett. **60**, 1490 (1988).
[9] N. Berrah, A. Farhat, B. Langer, B. M. Lagutin, Ph. V. Demekhin, I. D. Petrov, V. L. Sukhorukov, R. Wehlitz, S. B. Whitfield, J. Viefhaus, and U. Becker, Phys. Rev. A **56**, 4545 (1997).
[10] S. Alitalo, A. Kivimäki, T. Matila, K. Vaarala, H. Aksela, and S. Aksela, J. Electron Spectrosc. Relat. Phenom. **114**, 141 (2001).
[11] A. Caló, S. Sankari, A. Kivimäki, H. Aksela, and S. Aksela, J. Phys. B **39**, 4169 (2006).
[12] V. L. Sukhorukov, I. D. Petrov, B. M. Lagutin, A. Ehresmann, K. H. Schartner, and H. Schmoranzer, Phys. Rep. **786**, 1 (2019).
[13] S. Svensson, N. Mårtensson, E. Basilier, P. A. Malmquist, U. Gelius, and K. Siegbahn, Phys. Scr. **14**, 141 (1976).
[14] M. Ohno and G. Wendin, Phys. Scr. **16**, 299 (1977).
[15] M. Ohno and G. Wendin, J. Phys. B **11**, 1557 (1978).
[16] E. J. McGuire, Phys. Rev. A **5**, 1043 (1972).
[17] V. Schmidt, Z. Phys D **2**, 275 (1986).
[18] C. King, M. Tronc, F. H. Read, and R. C. Bradford, J. Phys. B **10**, 2479 (1977).
[19] H. Aksela, S. Aksela, and H. Pulkkinen, Phys. Rev. A **30**, 2456 (1984).
[20] F. A. Parpia, C. F. Fischer, and I. P. Grant, Comput. Phys. Commun. **94**, 249 (1996).
[21] S. Fritzsche, J. Electron Spectrosc. Relat. Phenom **114**, 1155 (2001).
[22] S. Fritzsche, Comput. Phys. Commun. **183**, 1525 (2012).
[23] C. F. Fischer, T. Brage, and P. Jönsson, *Computational Atomic Structure: An MCHF Approach* (Institute of Physics Publishing, Bristol, 1997).
[24] M. Borst and V. Schmidt, Phys. Rev. A **33**, 4456(R) (1986).
[25] J. Jauhiainen, A. Kivimäki, S. Aksela, O.-P. Sairanen, and H. Aksela, J. Phys. B **28**, 4091 (1995).
[26] B. Kammerling, A. Hausmann, J. Liuger, and V. Schmidt, J. Phys. B **25**, 4773 (1992).
[27] S. Fritzsche, J. Nikkinen, S. M. Huttula, H. Aksela, M. Huttula, and S. Aksela, Phys. Rev. A **75**, 012501 (2007).